Anomalous inelastic neutron scattering from calcite

1992 J. Phys.: Condens. Matter 4 2761

(http://iopscience.iop.org/0953-8984/4/11/006)

J. Phys.: Condens. Matter 4 (1992) 2761–2774. Printed in the UK

Anomalous inelastic neutron scattering from calcite

M T Dove†, M E Hagen‡§, M J Harris†¶, B M Powell||, U Steigenberger‡ and B Winkler†*

† Department of Earth Sciences, University of Cambridge, Cambridge CB2 3EQ, UK
‡ ISIS Facility, Rutherford Appleton Laboratory, Chilton, Didcot, Oxon OX11 0QX, UK
§ Department of Physics, Keele University, Keele, Staffs ST5 5BG, UK
|| Chalk River Laboratories, AECL Research, Chalk River, Ontario KOJ 1JO, Canada

Received 14 October 1991, in final form 23 December 1991

Abstract. Inelastic neutron scattering measurements on calcite ($CaCO_3$) in its low temperature phase have revealed the existence of an unusual column of inelastic scattering at the wavevector corresponding to the F point of the high temperature Brillouin zone. At the same wavevector there is also a transverse acoustic soft mode and the column of scattering ranges in energy from zero up to the soft mode. The intensity of the anomalous scattering increases rapidly with temperature, and is consistent with an Arrhenius relation of the form $\exp(-T^*/T)$, where $T^* = 1035$ K. We speculate that this scattering arises from thermal fluctuations of the calcite structure into a different ordered structure, which is related to an ordering instability at the F point. Evidence for this possibility has also been obtained from lattice energy calculations.

1. Introduction

Calcite, $CaCO_3$, undergoes an orientational order–disorder phase transition at 1260 K [1] which is similar to the more widely studied transition in sodium nitrate, $NaNO_3$ [2, 3, 4]. The carbonate ions in the high temperature phase (space group $R\bar{3}m$) are disordered with respect to 60° rotations about their 3 fold axes. In the low temperature phase (space group $R\bar{3}c$) the carbonate ions in a single (0,0,1) plane (indexed on the basis of a hexagonal unit cell) have identical orientations, but the ions in neighbouring planes are rotated by 60°. This corresponds in a diffraction experiment to the appearance of a superlattice reflection at the Z point of the high temperature Brillouin zone. The intensity of this superlattice reflection is proportional to the square of the order parameter Q for the transition [5]. In both calcite [1] and $NaNO_3$ [2] diffraction experiments have shown a temperature dependence for the order parameter of the form

$$Q = Q_0|T_c - T|^\beta \tag{1}$$

where $\beta = 0.25$. As an aside we note that in $NaNO_3$, but not in calcite, the value of β is lowered to 0.22 close to the transition temperature [2]. A value of $\beta = 0.25$ is consistent with a three-dimensional tricritical phase transition. This type of transition

¶ Present address: Oxford Physics, Clarendon Laboratory, Parks Road, Oxford OX1 3PU, UK.
* Present address: Laboratoire Leon Brillouin, CEN Saclay, 91191 Gif-sur-Yvette, Cedex, France.

0953-8984/92/112761+14$04.50

occurs when the co-efficient of the fourth-order terms in the Landau expansion of the free energy are 'accidentally' zero [5]. The reason why this tricritical exponent value should apply to both systems is therefore not fully understood at this time. As a result of the diffraction work on $NaNO_3$ it has been suggested that there is a competing ordering scheme, which may not necessarily give rise to a new phase at any temperature, but which will affect the thermodynamic behaviour in such a way that it gives rise to tricritical behaviour [2]. It is believed that this ordering scheme involves an instability at the F point of the Brillouin zone of the high temperature disordered phase, which is the $(\overline{1}/2,0,2)$ point in the reciprocal lattice of the low temperature phase (note that we use the convention for Bragg vectors that $h + k + l = 3n$). In figure 1 the a^*–c^* section of reciprocal space is shown with the Z and F points marked along with the Brillouin zones of both high and low temperature phases. The primed labels in this figure refer to the low temperature phase. Strong diffuse scattering is observed at F points along the line passing through the (0,0,12) and (3,0,0) zone centres in x-ray diffraction photographs of both calcite (at room temperature) and $NaNO_3$ (close to T_c) [6]. Since the actual low temperature order involves an instability at the Z point of the reciprocal lattice of the high temperature phase, which is the (0,0,3) point in the low temperature structure, we therefore denote the observed low temperature structure as the Z phase.

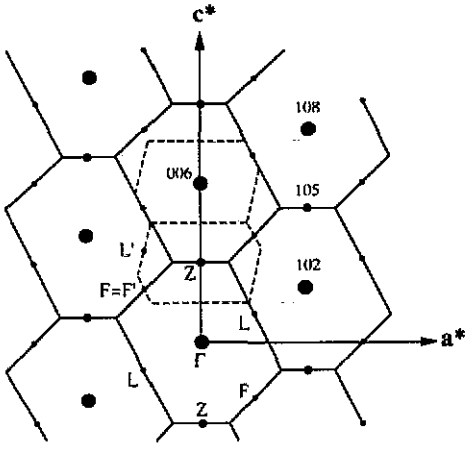

Figure 1. The a^*–c^* plane of reciprocal space, with Bragg vectors of the ordered Z phase indicated. The full lines mark the Brillouin zone of the disordered form, and the broken lines mark the Brillouin zone of the ordered Z form. Note that the L' and F' points marked apply to the low temperature Brillouin zone while the points marked L and F apply to the high temperature zone.

In order to investigate the origin of the diffuse scattering in calcite, we have performed inelastic neutron scattering measurements of the low energy phonon dispersion curves along the direction Γ to F. These measurements have been carried out using triple axis spectrometers at the NRU reactor at Chalk River Laboratories, Canada, and the PRISMA spectrometer at the ISIS spallation neutron source, Rutherford Appleton Laboratory, UK. The experimental procedure used during these measurements is described in section 2, and the results are presented in section 3.

There have been some previous inelastic neutron scattering studies of both calcite and $NaNO_3$. A study of the phonon dispersion curves along the c^* axis in calcite was

reported by Cowley and Pant [7]. For $NaNO_3$ the dispersion curves along the c^* axis at room temperature and the temperature dependence of some of the zone centre optic modes has been measured by Lefebvre *et al* [8]. A brief report of a study of the lowest energy TA mode at the F point in $NaNO_3$ has recently been given by Schmahl *et al* [9].

We also report in this paper calculations of the lattice energy of calcite and of the phonon dispersion curves using an interatomic potential model developed by Dove *et al* [10]. This model uses short range interactions for non-bonded contacts, and bond-bending and torsional interactions to represent the flexibility of the carbonate molecular ion. The calculated dispersion curves for the direction Γ–F are compared with our measurements in section 3. In section 4 the model is used to calculate the energies of different possible ordered structures of calcite. The use of potential functions means that the expected agreement between calculated and observed dispersion curves is not as good as for force constant models, but does allow the calculation of the energies of different structures. The model was not optimised against any data obtained in the present study.

2. Experimental methods

The triple axis spectrometer measurements were performed at the NRU reactor, Chalk River, on the C5 and N5 spectrometers. The crystal used in these room temperature measurements had a volume of 10 cm^3 and was aligned with a $[0,\bar{1},0]$ axis vertical. The initial triple axis measurements of the phonon dispersion relations were performed in a constant-Q mode with a fixed final neutron energy of 14.5 meV. Later measurements of the inelastic scattering observed around the F point at (2.5,0,2) were performed in a constant-E mode. Most of these latter measurements were performed with a fixed final neutron energy of 14.5 meV although some high resolution data were collected with a lower final neutron energy of 11.6 meV. The monochromator and analyser crystal planes used were silicon (1,1,3) and pyrolitic graphite (0,0,2) reflections, respectively. In the monochromator to sample, and sample to analyser positions, the collimations were, respectively, 0.6° and 0.4°. The majority of the measurements performed were for wavevectors along the direction from (0,0,12) to (3,0,0) but some measurements were also made along different directions in the a^*–c^* plane away from the F point at (2.5,0,2).

Measurements as a function of temperature were performed using the PRISMA spectrometer at ISIS. This is a multi-analyser indirect geometry time of flight spectrometer and it has recently been described in detail by Steigenberger *et al* [11]. The measurements were performed using germanium (1,1,1) analyser crystals with negative ϕ and $2\theta_A$ scattering angles. The spectra on PRISMA are collected along a path in which both the wavevector transfer, Q, and energy transfer, E, vary. By exploiting the time of flight nature of the measurements a series of these paths can be measured simultaneously thereby enabling phonon dispersion relations to be mapped out. The single crystal used for the PRISMA experiments had a volume of 6 cm^3, and was mounted with a $[0,\bar{1},0]$ axis vertical. The spectra were collected along the $[1,0,\bar{4}]$ direction through the (3,0,0) zone centre. A closed cycle refrigerator (CCR) was used for cooling the sample and a vacuum furnace for heating. The temperature in the CCR was measured using a rhodium–iron resistance thermometer and in the furnace a K-type (nickel–chromel) thermocouple was used. A temperature stability of

better than ± 1 K was maintained throughout the measurement period of each run. The measurements in the furnace were restricted to an upper temperature limit of 800 K in order to remain well below the temperature for the decomposition reaction $CaCO_3 \rightarrow CaO + CO_2$ [1]. For the measurements below 500 K the crystal was held by an aluminium frame. This was replaced by a stainless steel frame for temperatures above 500 K. Unfortunately this lead to some spurious peaks arising from powder lines in the steel in some of the spectra which were not present when the aluminium frame was used.

3. Experimental results

3.1. Dispersion curves from triple axis spectrometer results

The dispersion curves for Γ–F obtained from our constant-Q data taken on C5 at Chalk River are shown in figure 2(a). The most striking feature in this data is the softness of the transverse acoustic mode at the F point. This is partly due to anti-crossing interactions with other phonons of the same symmetry; note, there are only two irreducible representations for any general point in the a^*–c^* plane. These anti-crossing effects appear in our calculations of the dispersion curves which are shown in figure 2(b), but the size of the gap suggests that these interactions are not wholly responsible for the amount of softening. The measured dispersion surface about the F point for several directions in the a^*–c^* plane is shown in figure 3. It is clear that the soft mode at F is a true minimum in this plane, and our calculations show that it is a true minimum for all directions in reciprocal space away from F. It can also be seen that there is a marked anisotropy of the phonon dispersion for different directions about F, with the softest direction being that along Γ–F.

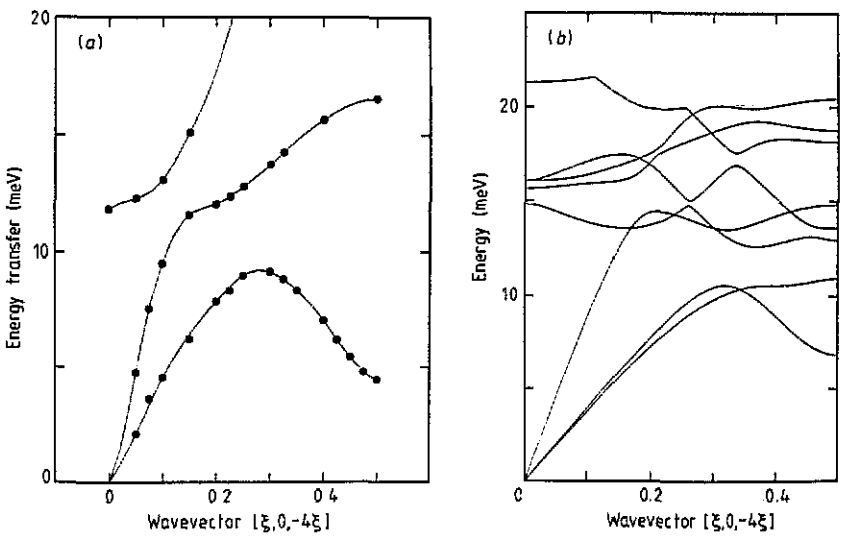

Figure 2. The low energy dispersion curves of calcite along the direction $[\xi, 0, \overline{4\xi}]$ from Γ ($\xi = 0$) to F ($\xi = 0.5$): (a) as measured at room temperature by inelastic neutron scattering at Chalk River (the full curves are guides to the eye), and (b) as calculated by Dove *et al* [10].

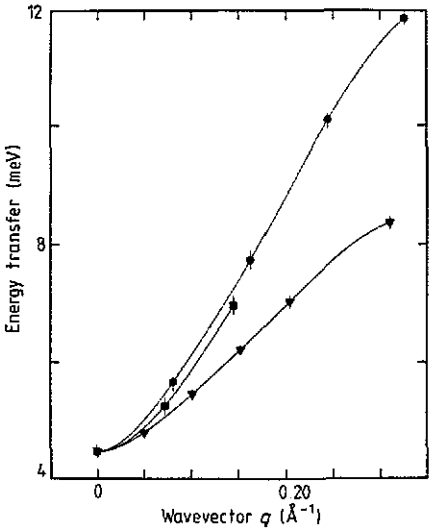

Figure 3. The dispersion of the soft phonon modes measured about the (2.5,0,2) position in the directions $[\xi,0,0]$ (●), $[\xi,0,\overline{4}\xi]$ (▲) and $[\xi,0,2\xi]$ (■).

3.2. PRISMA results for heating and cooling

Following the initial observation of the incipient soft mode at F using the triple axis spectrometer we investigated the temperature dependence of these phonon branches using the PRISMA spectrometer. The phonon dispersion relations measured at 10, 293, 373, 473, 573 and 773 K are shown in figures 4(*a*)–(*f*). The data shown in figures 4(*a*)–(*f*) are the result of combining two (373, 573 and 773 K) or three (10, 293 and 473 K) runs on PRISMA. Each run consisted of 13 spectra and took about 8–12 hours to collect with ISIS running at a proton current of 100 μA. In figures 4(*a*)–(*f*) the full curves are merely guides to the eye, which have been determined from the room temperature data. These guides are the same in different reduced zones and in neutron energy gain as well as loss. They are also the same as those shown in figure 2(*a*) for the triple axis data and as a consequence it can be seen from figures 2(*a*) and 4(*b*) that the room temperature PRISMA and triple axis data are consistent for all points except that at $\approx$ 17 meV. The incipient soft mode at the F point in the PRISMA data is a prominent feature just as it was in the triple axis data. It should be noted that the guides shown in figures 4(*a*) and 4(*c*)–(*f*) are the same room temperature guides as in figure 4(*b*). This has been done to emphasize the fact that, except at the F point there is little change in the phonon dispersion relations with temperature. The broken curves in figures 4(*a*)–(*f*) indicate the path in Q–E space corresponding to one of the spectra measured, which in this case passes through $E = 0$ at the $Q = (2.5, 0, 2)$ F point. The spectra measured along this path at each of the temperatures from 10 to 773 K are shown in figures 5(*a*)–(*f*).

The PRISMA results showed a feature which had not been previously noted in the triple axis measurements. At (2.5,0,2) for the temperatures from 293 to 773 K there is an anomalous column of scattering that rises from zero energy up to the energy of the incipient soft transverse acoustic branch. In figures 4(*b*)–(*f*) this is shown by the vertical line of data points representing the peak positions measured in the spectra from different detectors. In figures 6(*a*)–(*f*) we show, as an example,

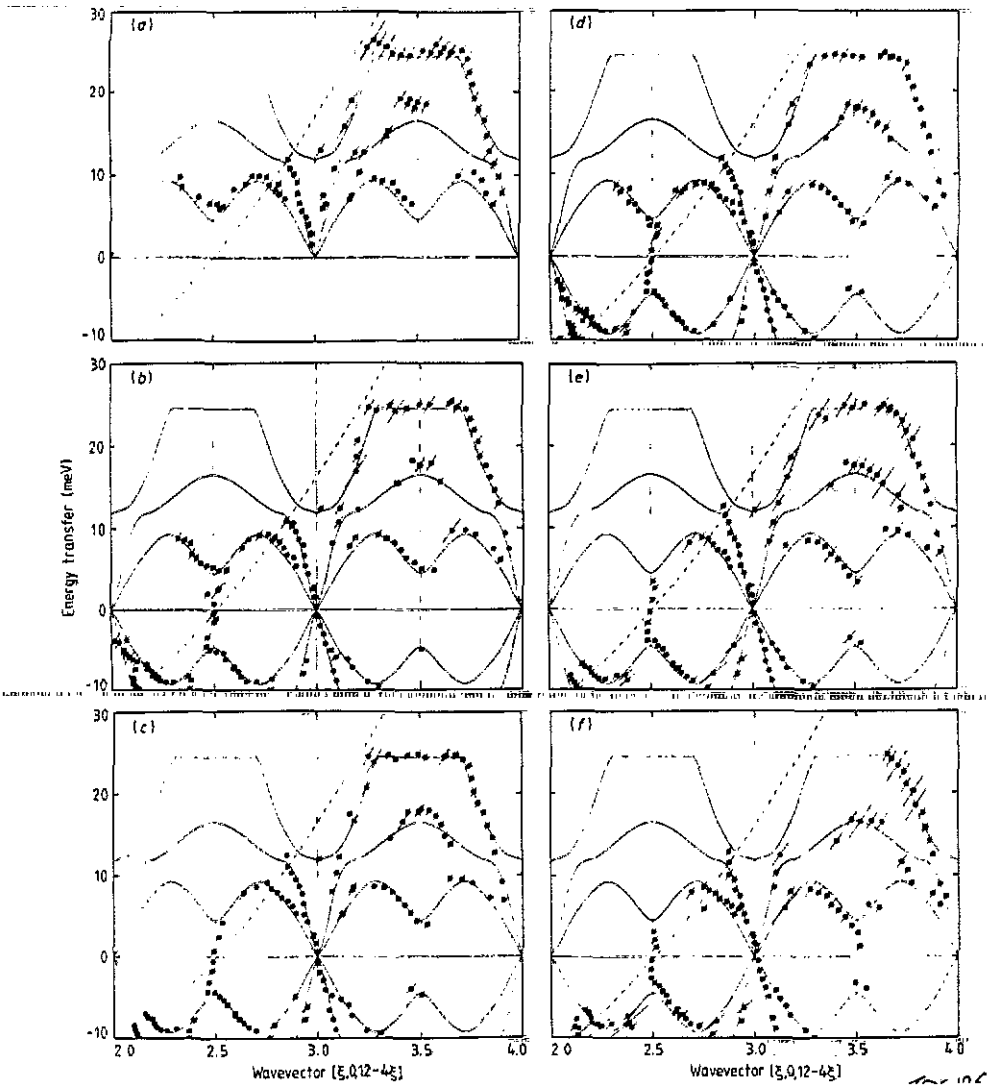

Figure 4. The dispersion curves along the $[\xi,0,4\overline{\xi}]$ direction through the (3,0,0) Bragg peak measured at the following temperatures: (*a*) 10 K, (*b*) 293 K, (*c*) 373 K, (*d*) 473 K, (*e*) 573 K, and (*f*) 773 K using the PRISMA spectrometer. The points indicate the positions of the peaks in the individual spectra and the error bars are oriented in the direction of the Q–E trajectories of the individual detectors. The full curves are guides to the eye constructed from the data of figure 2 for the lower branches and from the PRISMA data at 293 K for the upper branch. The broken curves indicate the Q–E trajectory of the detector whose spectra are shown in figure 5.

how this column of scattering is manifested in the time of flight spectra at 473 K. A single run on PRISMA produces spectra along a series of successive Q–E paths, one for each detector. An example of such a series of paths is given in figure 7 of [11]. The spectra shown in figures 6(*a*)–(*c*) correspond to detectors 1, 2, and 3, that shown in figure 4(*d*) to detector 4, and those in figures 6(*d*)–(*f*) to detectors 5, 6, and 7. The arrows in figures 6(*a*)–(*f*) indicate the positions of the column of scattering in

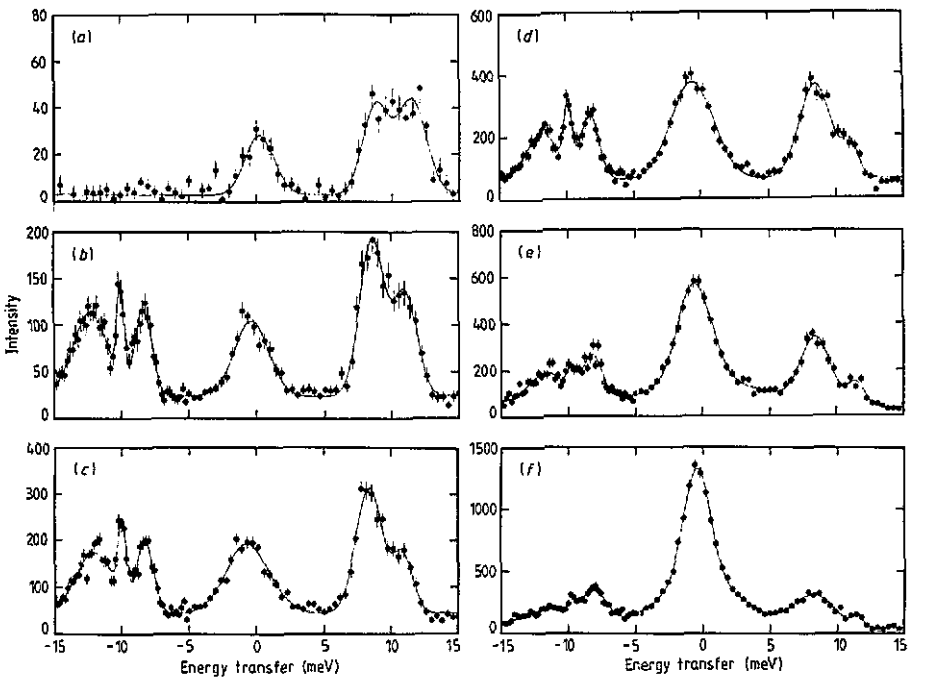

Figure 5. The spectra (note, figures (a)–(f) denote the same temperatures as in figure 4) for the detector whose Q–E trajectory is indicated by the broken curves in figures 4(a)–(f).

each spectra.

Another way of looking at the data in this region of reciprocal space is to select the data from different spectra correponding to the same wavevector transfer, in effect to extract a constant-Q scan from the time of flight data set. In figures 7(a)–(f) we show the data extracted in such a manner for each of the temperaures from 10 to 773 K at the wavevector $Q = (2.5, 0, 2)$. A comparison of the data in figures 4(b), 5(b) and 6(b) shows that the anomalous scattering at the F point is in fact a column of scattering, narrow in wavevector but extended in energy between zero energy and the soft phonon.

Despite numerous calculations, we have been unable to invoke any spurious process that can explain this anomalous scattering and we therefore regard it as a real effect. The most convincing attribute of the scattering at (2.5,0,2) and that which is probably the clearest indication of its origin is the dramatic temperature dependence of its intensity which is most clearly shown in figures 5(a)–(f). At 10 K the scattering is absent from both neutron energy loss and energy gain, the small peak at $E = 0$ in figure 5(a) is consistent with the incoherent elastic line measured at other wavevectors. However, at 773 K the anomalous scattering has become the dominant feature in the spectrum as can be seen from figure 5(f). In the temperature range from 293 to 773 K the intensity of the phonon peaks shown in figures 5(b)–(f) has risen by a factor of ≈ 2 consistent with the Bose population factor, while the scattering observed at $E = 0$ has grown in intensity by a factor of ≈ 14. These measurements were found to be both reversible and reproducible with both temperature and time.

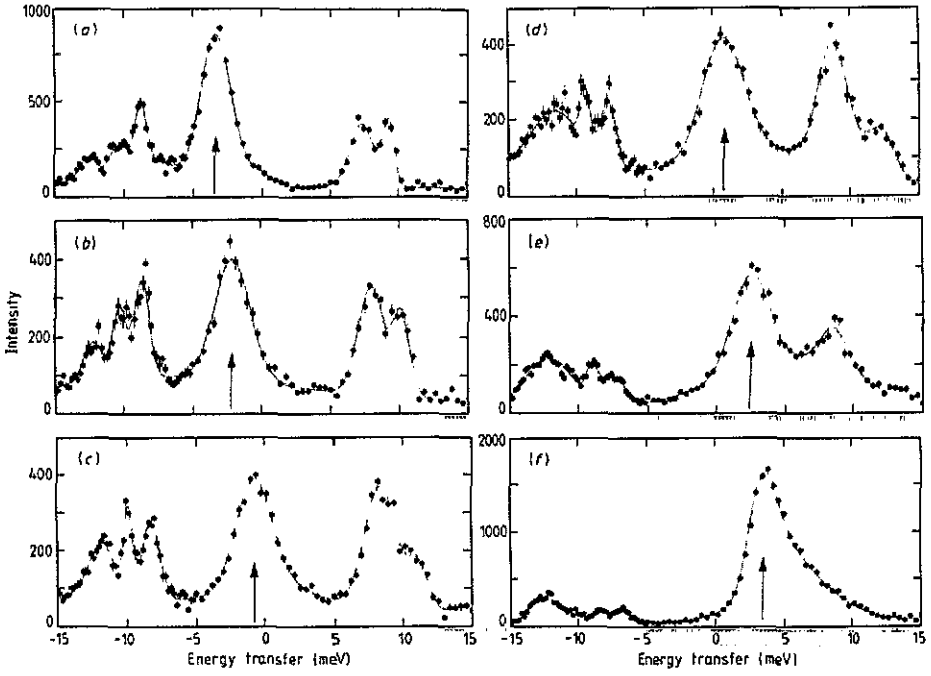

Figure 6. The spectra from 6 detectors measured at 473 K on PRISMA. The peaks indicated by the arrows are those given by the column of anomalous scattering at the F point, which are shown as points at (2.5,0,2) in figure 4(*d*).

The constant-Q extractions shown in figures 7(*a*)–(*f*) show that although at room temperature we can identify a column of scattering which is independent of the lineshape of the soft phonon mode, at higher temperatures such a distinction is not so clear. The energy of the soft mode decreases with increasing temperature and there is obviously an interaction with the anomalous column of scattering. Since we are limited to temperatures below 800 K (which is only 0.65 of T_c) it is difficult to draw any conclusions as to how low in energy the soft mode will fall. However, it does appear to be softening faster than in $NaNO_3$ [9]. The temperature dependence of the energy at which the intensity of the soft phonon peaks, as deduced from the plots in figures 7(*a*)–(*f*), is shown in figure 8. It should be noted that away from the F point the transverse acoustic phonons appear as well defined peaks, with no damping, in both the time of flight spectra and in constant-Q extractions at all temperatures up to 773 K.

3.3. Further triple axis spectrometer results

Following the discovery of the anomalous column of scattering at the F point we performed further room temperature measurements using the N5 triple axis spectrometer at Chalk River Laboratory, this time operating in a constant-E mode. A number of spectra scanning along the Γ–F direction through (2.5,0,2) for various energy transfers from zero up to the soft mode energy were performed. An example of one of these scans for an energy transfer of 2.48 meV, which is mid-way between zero and the energy of the soft-phonon, is shown in figure 9. By changing the analysing

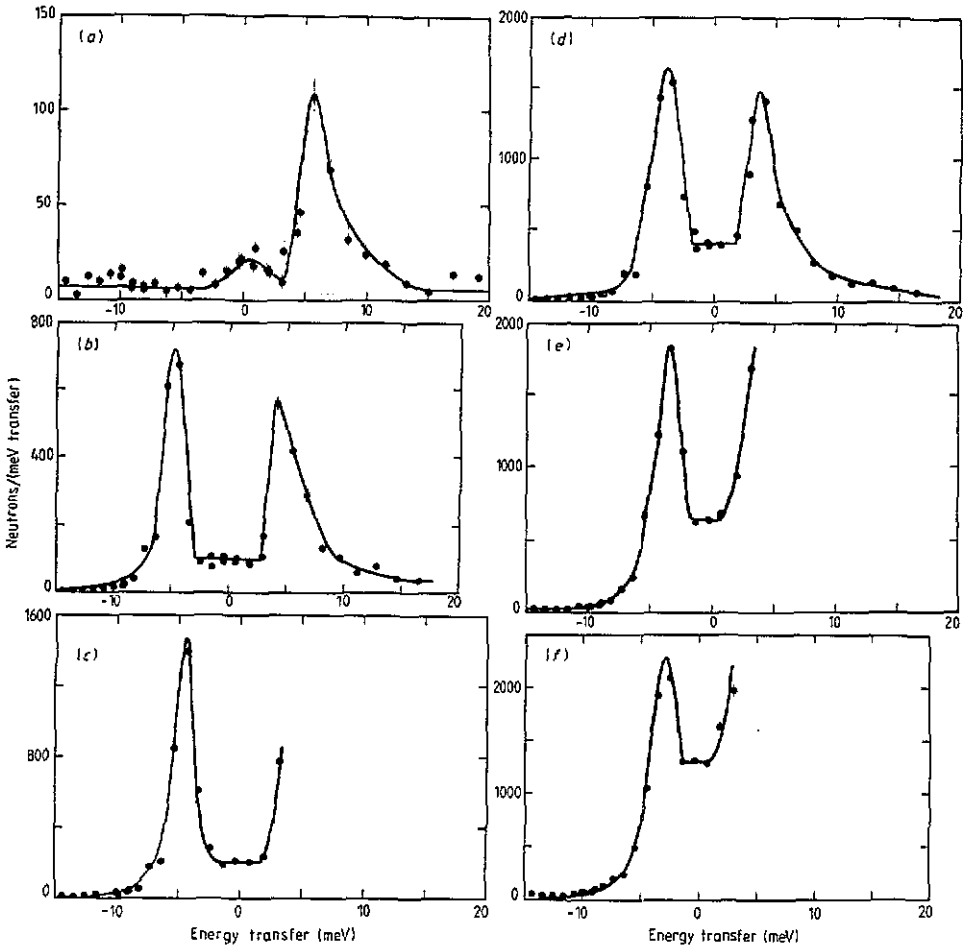

Figure 7. The spectra shown at (*a*) 10 K, (*b*) 293 K, (*c*) 373 K, (*d*) 473 K, (*e*) 573 K, and (*f*) 773 K are constant-Q extractions from the set of time of flight spectra.

energy of the triple axis spectrometer to 11.6 meV we were able to show that the scattering shown in figure 9 is not limited by the wavevector resolution of the spectrometer and have deduced a linewidth in the wavevector of ≈ 0.01 Å^{-1}. A series of measurements were also performed to examine how the intensity of this anomalous scattering varied for different F points. We note from figures 4(*a*)–(*f*) that it appears to be absent at the (3.5,0,2) F point. From an examination of the F points within a radius of 4.40 Å^{-1} we have found that the intensity is strongest at (2.5,0,2) and is only significant at F points on the line passing through (0,0,12) and (3,0,0).

4. Discussion

The main question arising from the work reported in this paper concerns the origin of the scattering observed at the F point. We believe that it must be associated with the ordering phase transition, almost certainly as a result of the competition between different ordering schemes. The integrated intensities of the scattering at the F point

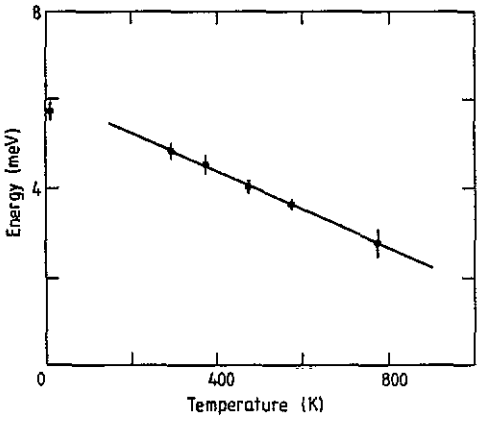

Figure 8. A plot of the temperature dependence of the energy at which the intensity of the soft phonon at (2.5,0,2) peaks (cf. figures 7(*a*)–(*f*)).

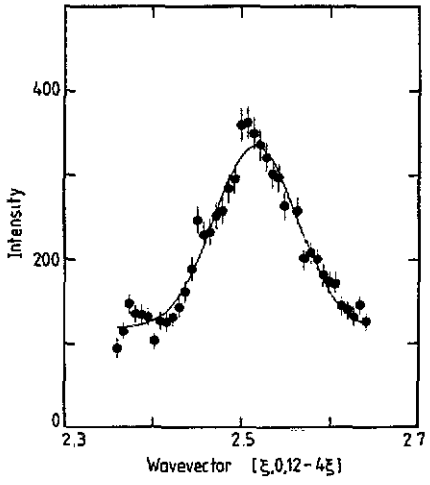

Figure 9. A constant-E spectrum measured at room temperature along the $[\xi,0,\overline{4\xi}]$ direction through (2.5,0,2) at an energy transfer of 2.48 meV which is mid-way between zero and the soft phonon energy using the N5 triple axis spectrometer.

(not including that from the main phonon peak) are consistent with an Arrhenius relation of the form

$$I = Ak_{\mathrm{B}}T\exp(-T^{*}/T) \tag{2}$$

where the factor of $k_{\mathrm{B}}T$ accounts for the thermal population (in the classical approximation) and A is a constant of proportionality. The data are best fitted with an activation temperature $T^{*} = 1035$ K (corresponding to an activation energy of 0.089 eV). In figure 10 we show a plot of the integrated intensities divided by $k_{\mathrm{B}}T$ against temperature where the full curve is the best fit to equation (2).

The scattering we have observed in calcite is similar to that observed in BCC β-Ti [12, 13], where a column of inelastic scattering was observed at the wavevector of an incipient soft mode. In β-Ti the soft mode is associated with the unstable ω

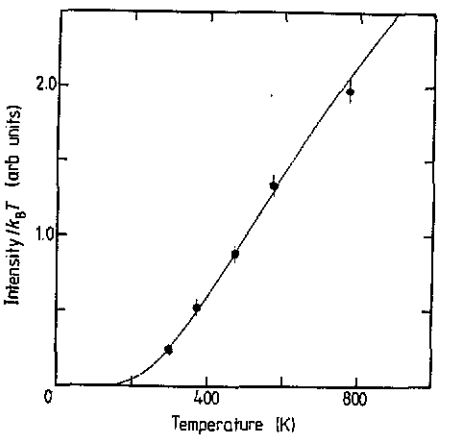

Figure 10. A plot of the temperature dependence of the integrated intensity of the anomalous scattering at the F point divided by the population factor, k_BT. The full curve is the fit to the Arrhenius relation as described in the text.

phase, which sometimes appears as a metastable phase and which could be formed by the condensation of the incipient soft mode. As a consequence this effect has been interpreted as being due to fluctuations of small domains of the BCC phase into the ω phase. In the case of calcite we can invoke a similar explanation for the scattering we have observed. It should be noted, however, that the effect in calcite has been found in the low temperature phase whereas in BCC Ti it has been found in the high temperature 'disordered' phase.

If there are a number of possible ordering structures that are accessible from the disordered phase, it is likely that some of these will have similar energies and that it ought to be possible for small regions of the equilibrium ordered phase to spontaneously fluctuate into one of the other possible ordered phases. In this case, we postulate that there is an ordered phase, which we will denote as the F phase, that corresponds to an ordering instability at the F point wavevector of the disordered phase. This may not be the only possible fluctuation accessible to the ordered structure, but it is likely to be the fluctuation responsible for the scattering we have observed at the F point. This explanation is consistent with the temperature dependence of the scattering as interpreted by an Arrhenius relation. The activation temperature T^* would then be related to the energy required for the Z phase to fluctuate into the F phase and the experimental value of $T^* = 1035$ K is consistent with this explanation (i.e., less than, but similar to, the transition temperature). This explanation is also (self-evidently) consistent with the absence of scattering at very low temperatures.

In order to provide some quantitative estimates of the energies required for fluctuations into the F phase we have performed lattice energy calculations using the model for calcite of Dove *et al* [10]. The equilibrium Z and F structures calculated using this interatomic potential model are compared in figure 11 and table 1. The calculated Z structure is only negligibly different from that observed at room temperature. The starting point for the F structure (monoclinic space group $P2/a$ with 2 formula units per unit cell, and not $P2_1/c$ as mistakenly stated in [4]) was taken from the work of Lynden-Bell *et al* [3]. The main difference between the Z and F structures is that in the F structure alternate $(1,0,\bar{4})$ planes of carbonate

Table 1. (*a*) Calculated cell parameters, volume per formula unit (V) and energy per formula unit (E), for the Z and F phases. (*b*) Fractional atomic co-ordinates of the calculated F phase for space group $P2/a$.

(*a*)

	Z	F
a (Å)	4.9822	8.7372
b (Å)	4.9822	4.9635
c (Å)	17.3264	6.6146
α (°)	90.0	90.0
β (°)	90.0	153.452
γ (°)	120.0	90.0
V (Å^3)	62.08	64.10
E (eV)	−34.38	−34.31

(*b*)

Atom	x	y	z
Ca	0.25	0.3176	0.5
C	0.25	−0.1780	0.0
O1	0.25	0.0808	0.0
O2	0.3742	−0.3084	−0.004

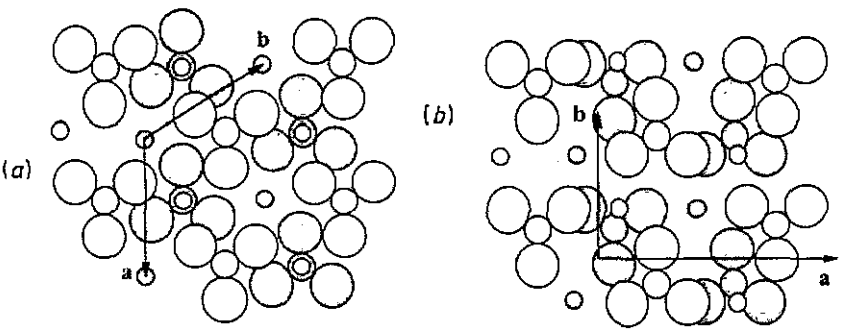

Figure 11. The calculated structures of the Z and F phases, viewed down a common direction (c for the Z phase and c^* for the F phase), are shown in (*a*) and (*b*), respectively. The largest symbols represent oxygen, the intermediate size symbols represent carbon and the smallest symbols represent calcium. Two layers of carbonate groups are shown, the shaded ones being below the open ones. The layer of shaded calcium atoms is halfway between the two carbonate layers and the layer of open calcium atoms is a similar distance above the layer of open carbonate groups. Also shown are the a–b vectors of the respective structures centred on the origins of the unit cells.

ions are rotated by 60° with respect to the Z structure. To lower the energy these rotations are accompanied by small displacements along the [0,1,0] direction of the F structure. This coupling between rotation and displacement has been studied in detail by Lynden-Bell *et al* [3]. The volume per formula unit of the F phase is calculated to be about 3 % larger than that of the Z phase, and the energy per formula unit of the F phase is calculated to be about 0.072 eV higher than that of the Z phase. Since these are zero temperature calculations the effect of entropy is neglected. The calculated value is less than the energy of 0.1 eV determined by Redfern *et al* [14] for the transition from the Z phase to the disordered paraphase at zero temperature. We can therefore conclude that the F structure is accessible as a thermal fluctuation of the Z structure. The calculated energy difference of 0.072 eV between the two phases is quite close to the measured activation energy of 0.089 eV suggesting that we are indeed observing this fluctuation.

The model can also shed light on the observation of additional peaks in the infrared absorption spectra of $NaNO_3$ at temperatures close to its transition temperature

Table 2. Frequencies of the high energy internal modes of carbonate and nitrate molecular ions for the Z and postulated F phases of calcite $NaNO_3$. The calculated frequencies are given in brackets for calcite. The data for the F phase of $NaNO_3$ are the additional peaks observed in the Raman and infra-red spectra. Only transverse modes are given here and the units are cm^{-1}.

	ν_1	ν_2	ν_3	ν_4
Distortion	Symmetric stretch	Out-of-plane vibration	Asymmetric stretch	Asymmetric stretch (bend)
Calcite Z	1088 § (1049)	881 § (809)	1465 § (1469)	714 §(704)
Calcite F	(1029)	(805)	(1429–1448) ‖	(677, 702) ‖
$NaNO_3$ Z †	1068	836	1378	726
$NaNO_3$ F †	1063	826	$\approx$ 1340, $\approx$ 1480 ‡	—

† Experimental data for $NaNO_3$ are taken from [4, 15, 16, 17, 18]. No additional peaks associated with the ν_4 mode in $NaNO_3$ have been reported, probably due to the weak intensity of this mode.

‡ We identify the weak shoulder at $\approx$ 1340 cm^{-1} with the F phase, and the stronger shoulder at $\approx$ 1480 cm^{-1} with another thermally activated phase.

§ Experimental data for calcite are taken from [19].

‖ Different values are given since the exact frequency depends upon the direction of the wavevector.

[4, 15, 16, 17, 18] which are associated with internal vibrations of the nitrate molecular ions. We have calculated the energies of the internal modes of the carbonate ions in both the Z and F ordered structures of calcite (which are given in table 2) and have shown that the energy shifts between the two phases match the energy shifts observed in $NaNO_3$. We can therefore interpret most of the additional peaks observed in $NaNO_3$, namely those with lower energies than the main peaks, as arising from internal modes of the nitrate ions that are within domains of the F phase that have been thermally excited on heating. The additional ν_3 peak observed at $\approx$ 1480 cm^{-1} is not, however, explained by these calculations and we believe that it arises from fluctuations into other (as yet unobserved) ordered structures.

We conclude by noting that if the Z phase spontaneously fluctuates into the F phase (and possibly into other phases), the order parameter for Z phase ordering will be lowered at higher temperatures. This is different from fluctuations into either random disorder (as assumed in a mean field theory) or into domains of negative order (as in the cluster model of an array of Ising spins). We therefore speculate that it is these fluctuations which are responsible for the tricritical value of the critical exponent β.

We believe that our results may have implications for other order–disorder phase transitions in which competing ordering schemes may exist. One example is ice, where many different ordered structures can be constructed which are consistent with the constraints on hydrogen bonding. Another example is the Al/Si cation ordering in the mineral leucite, $KAlSi_2O_6$, which remains disordered at low temperatures. In this example, the simple ordering pattern suggested by the symmetry of the structure, which a Bragg–Williams model predicts should occur at about 2000 K, never occurs because of the existence of a large number of competing ordering schemes which destroy the ordering at high temperatures.

Acknowledgments

We thank Dr S M Hayden, Dr R Lynden-Bell and Dr W Schmahl for the helpful discussions we have had with them on different aspects of the work reported here. We are also grateful for the assistence provided by Ian Bailey and Andrew Chappell with the sample environment equipment at ISIS. One of us (MJH) acknowledges the receipt of an NERC studentship during the course of this work. The financial support of the SERC, at the ISIS Facility and in providing the travel funds for one of us (MTD) to carry out work at Chalk River, is gratefully acknowledged. Chalk River Laboratories are operated by AECL Research and we are grateful for their provision of beam time and for the hospitality of the staff at Chalk River.

References

[1] Dove M T and Powell B M 1989 *Phys. Chem. Minerals* **16** 503
[2] Schmahl W W and Salje E 1989 *Phys. Chem. Minerals* **16** 790
[3] Lynden-Bell R M, Ferrario M, McDonald I R and Salje E 1989 *J. Phys. Condens. Matter* **1** 6523
[4] Harris M J, Salje E and Guttler B K 1990 *J. Phys. Condens. Matter* **2** 5517
[5] See for example, Bruce A D and Cowley R A 1981 *Structural Phase Transitions* (London: Taylor and Francis)
[6] Schmahl W W 1988 unpublished
[7] Cowley E R and Pant A K 1973 *Phys. Rev.* B **8** 4795
[8] Lefebvre J, Currat R, Fouret R and More M 1980 *J. Phys. C: Solid State Phys.* **13** 4449
[9] Schmahl W W, Pintchovius L and Fuess H 1989 *Zeit. für Krist.* **186** 261
[10] Dove M T, Winkler B, Leslie M, Harris M J and Salje E 1992 *Am. Mineral.* at press
[11] Steigenberger U, Hagen M, Caciuffo R, Petrillo C, Cilloco F and Sachetti F 1991 *Nucl. Instrum. Methods* B **53** 87
[12] Petry W, Flottmann T, Heiming A, Trampanau J, Alba M and Vogl G 1989 *Phys. Rev. Lett.* **61** 722
[13] Petry W, Heiming A, Trampenau J, Alba M, Schrober H R and Vogl G 1991 *Phys. Rev.* B **43** 10933
[14] Redfern S A T, Navrotsky A and Salje E 1989 *Contr. Petrol. Minerol.* **101** 479
[15] Brooker M H 1978 *J. Phys. Chem. Solids* **39** 657
[16] Chisler E V 1969 *Sov. Phys.–Solid State* **11** 1032
[17] Karpov S V and Shultin A A 1976 *Sov. Phys.–Solid State* **18** 421
[18] Prasad Rao A D, Katujun R S and Porto S P S 1971 *Adv. Raman Spectrosc.* **1** 174
[19] White W B 1974 *The Infra-red Spectra of Minerals* ed V C Farmer (London: Mineralogical Society Monographs)